Profile Evolution for Conformal Atomic Layer Deposition over Nanotopography

Erin R. Cleveland,[†,‡] Parag Banerjee,[†,‡] Israel Perez,[†,‡] Sang Bok Lee,[⊥,∥] and Gary W. Rubloff[†,§,*]

[†]Department of Materials Science and Engineering, [‡]Institute for Systems Research, [§]Institute for Research in Electronics and Applied Physics, and [⊥]Department of Chemistry & Biochemistry, University of Maryland, College Park, Maryland 20742, and [∥]Graduate School of Nanoscience and Technology (WCU), Korea Advanced Institute of Science and Technology, 335 Gwahangno, Yuseong-gu, Daejeon 305-701, Korea

ABSTRACT The self-limiting reactions which distinguish atomic layer deposition (ALD) provide ultrathin film deposition with superb conformality over the most challenging topography. This work addresses how the shapes (*i.e.*, surface profiles) of nanostructures are modified by the conformality of ALD. As a nanostructure template, we employ a highly scalloped surface formed during the first anodization of the porous anodic alumina (PAA) process, followed by removal of the alumina to expose a scalloped Al surface. SEM and AFM reveal evolution of surface profiles that change with ALD layer thickness, influenced by the way ALD conformality decorates the underlying topography. The evolution of surface profiles is modeled using a simple geometric 3D extrusion model, which replicates the measured complex surface topography. Excellent agreement is obtained between experimental data and the results from this model, suggesting that for this ALD system conformality is very high even on highly structured, sharp features of the initial template surface. Through modeling and experimentation, the benefits of ALD to manipulate complex surface topographies are recognized and will play an important role in the design and nanofabrication of next generation devices with increasingly high aspect ratios as well as nanoscale features.

KEYWORDS: atomic layer deposition · porous anodic alumina · conformality · nanopetunias

Paralleling the trend in electronic devices, high surface area 3D architectures for applications in energy,[1,2] catalysis,[3,4] and sensors[5−7] are exploiting the benefits found in using nanoscaled structures with increasingly high aspect ratios. In exploiting these nanostructures, the 3D topography is perhaps even more complex and demanding than in conventional applications found in ULSI-based applications, such as those demonstrated in trench and stacked capacitors in DRAM devices,[8] barrier technology for copper metallization,[9] and gate dielectric deposition on planar Si[10] and Fin-FET geometries.[11] For example, Banerjee *et al.* recently demonstrated a novel metal−insulator−metal (MIM) nanocapacitor using a combination of self-limiting processes to build multilayered functional films and self-assembled nanotemplates with nanopores ~50 nm wide × 10 μm deep (aspect ratio = 200).[1] In these structures, a primary performance limitation was set by the geometry of the nanoporous template consisting of sharp asperities, leading to enhanced local electric fields and low field breakdown, which would ultimately limit energy storage density.[1] This example emphasizes the need for understanding and optimizing our ability to synthesize complex 3D nanostructures. Complex surface topographies consisting of high aspect ratios, sharp asperities, and nanoroughness significantly challenge the ability to conformally coat complex nanostructures using traditional physical vapor deposition (PVD) and chemical vapor deposition (CVD) techniques.[6,12,13] However, atomic layer deposition (ALD) offers high-quality films with atomic level thickness control and unprecedented uniformity and conformality in the most demanding 3D nanostructures.[14−16]

In this paper, we explore the evolution of surface profiles for ALD films deposited on a prototype of a topographically rough surface. We utilize highly scalloped Al templates formed by the removal of porous anodic alumina (PAA) membranes. PAA is a self-assembled, electrochemical templating technique that results in a highly dense close-packed hexagonal array of cylindrical nanopores on the surface of aluminum.[17] PAA naturally lends itself to many nanotechnology applications, such as a template for growing nanowires and nanotubes and for self-assembling these structures in parallel, periodic arrays used to fabricate catalysts membranes,[4,6] dye-sensitized solar cells,[18] batteries,[19] and sensors.[5,6] When the PAA film is etched off, a self-ordered, close-packed hexagonal array of nanodimples is left imprinted in the underlying aluminum surface (Figure 1).[20] Nearest neighbor dimples meet at sharp points, and the

*Address correspondence to rubloff@umd.edu.

Received for review May 7, 2010 and accepted July 09, 2010.

Published online July 14, 2010.
10.1021/nn1009984

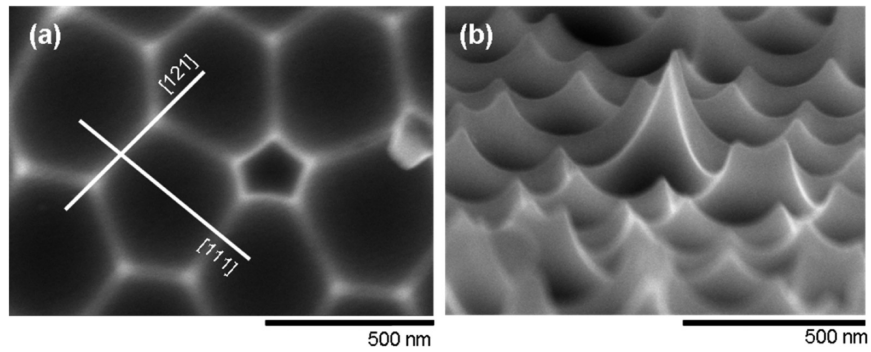

Figure 1. Removed PAA template imaged in SEM: (a) top-down view of the hexagonal nanodimple array displaying the [121] and [111] directions and (b) cross-section view of the scalloped Al surface, emphasizing the peak structure above the nanodimples.

overall surface topography consists of periodic peaks and valleys (Figure 1b). Due to aluminum's strong affinity for oxygen, the surface is coated with an amorphous native oxide.[21] Such surfaces are ideal for testing the influence of film conformality on surface nanotopography.

ALD is a self-limiting process which utilizes sequential chemisorbed surface reactions of precursor molecules to achieve deposition one monolayer at a time and is dependent upon molecule flux, adsorption/desorption probability, and surface diffusion.[22] Much work has focused on analytically understanding the performance of ALD conformality, particularly in high aspect ratio structures where process metrics (*i.e.*, reactant exposures and purge times) must be modified to compensate for the higher surface areas and molecular flow-type dynamics occurring in 3D nanostructures. This includes developing simple models for determining precursor dose for conformal coatings,[12] using Monte Carlo techniques,[14] solving simultaneously Boltzmann's transport and surface reaction equations[23] and correlating them with experimental results while trying to optimize conformality in ultrahigh aspect ratio structures. The prevailing message in the above reports is that ALD yields unparalleled performance when it comes to depositing thin films across complex 3D nanostructures but requires precise process control to ensure complete surface saturation and avoid excess deposition characteristic of CVD-like behavior.[22] On the other hand, the surface evolution of ALD films across complex surface topographies, especially with sharp asperities and nanoroughness, has not been systematically explored—experimentally or theoretically. Such complex topographies are still likely to incur complete saturation reactions and avoid topography-induced nucleation delays that could potentially affect the conformality of the films and the resulting topography.[22,24] Therefore, this work is aimed at investigating the surface evolution of ALD films in the context of highly scalloped surfaces.

Our test-bed utilizing a combination of a removed PAA membrane from an Al template and ALD provides us with the ability to monitor surface evolution of ALD films as they are deposited on a highly scalloped surface. We use two different templates with different interpore spacings (D_{int}) to reveal a universal behavior for the growth of ALD films on such surfaces following simple scaling laws. Furthermore, a surface extrusion model is used to verify this behavior and the resulting surface area as a function of ALD deposition thickness. This work demonstrates that through modeling and experimentation the benefits and limitations of ALD can be realized for complex nanostructures. Understanding this behavior will play a crucial role in the design and nanofabrication of next generation energy devices with increasingly high aspect ratios as well as nanoscale feature sizes.

RESULTS AND DISCUSSION

The evolution of ALD surface profiles over complex nanotopography was investigated with particular focus on how ALD modifies surface topography. PAA membranes formed in phosphoric acid with a D_{int} of 450 nm were removed from the underlying aluminum surface, revealing a highly textured surface of peaks and valleys that rise above an array of hexagonal dimples as seen *via* cross-sectional SEM (Figure 1a,b). Peaks are seen positioned along the [121] direction of the template, whereas valleys are found to traverse the [111] direction. Peak structures are multifaceted in shape due to the convergence of multiple hexagonal dimples. Peaks that rise notably above the average peak height and nonhexagonal dimples are considered defects. Defects are preferentially found along domain boundaries and are generally created during the anodization process when starting from a completely disordered structure, as opposed to a stamped template where the ordering is considered perfect.[25]

Templates formed in phosphoric acid were coated with three consecutive layers of 1000 cycle TiO_2 ALD. Top-down SEM images display surface profiles of TiO_2 ALD deposited on the scalloped Al surface after 0, 1000, 2000, and 3000 cycles (Figure 2a−d). Images reveal that increased ALD deposition results in the formation

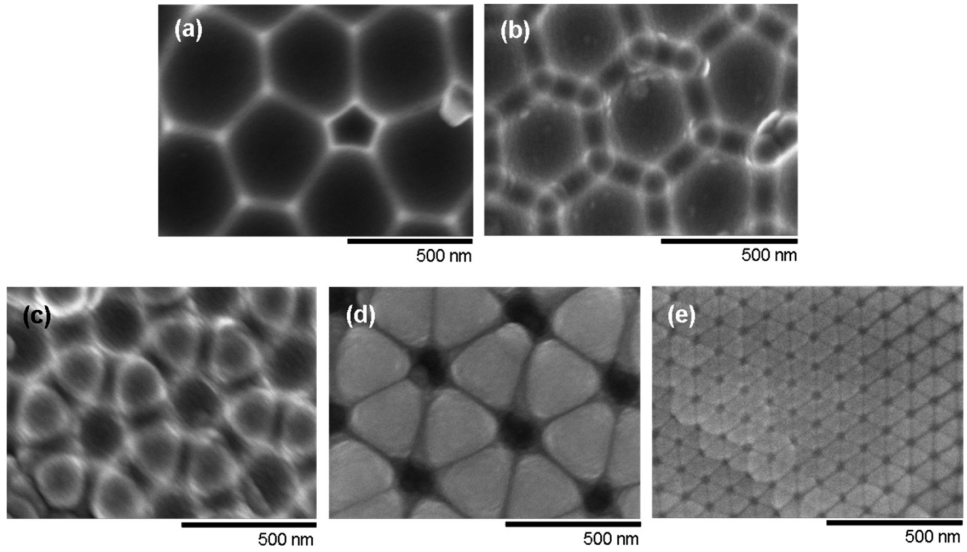

Figure 2. Progression of TiO_2 ALD profiles across a scalloped Al surface formed using phosphoric anodizing acid imaged in SEM after (a) 0, (b) 1000 (~55 nm), (c) 2000 (~110 nm), and (d) 3000 cycles (~165 nm). (e) SEM image of a scalloped Al surface using oxalic anodizing acid coated with 733 cycles (~40 nm) of TiO_2. Top-down images (d,e) display the same formation of triangular ALD surface profiles for the same ratio of equivalent thickness (t) to interpore spacing distance (D_{int}) for each anodizing acid.

of triangular patterns originating from the peak structures across the surface. In Figure 2b, it appears that ALD deposition is nucleating at these sharp tips, thus dominating ALD growth across the surface and creating areas of higher growth over others, as seen in Figure 2c. As deposition continues, growth fronts originating from these peaks start to merge and exhibit symmetric, repeating patterns of raised triangles decorating the surface with "nanopetunias", as seen in Figure 2d.

A simple scaling law was devised to adequately compare the ALD surface profiles deposited on templates formed with different interpore spacing using either phosphoric or oxalic acid. Using the film's growth rate, deposition on one template could be scaled by a factor of k defined in eq 1 as

$$k = t/D_{int} \quad (1)$$

where t is the measured film thickness for a set number of cycles deposited on planar surfaces, in order to calculate an equivalent film thickness (τ) for a template with a different interpore spacing (D^{o}_{int}). Leaving $\tau = kD^{o}_{int}$. SEM images display templates produced with different interpore spacings of 450 nm for phosphoric acid (Figure 2d) and 110 nm for oxalic acid (Figure 2e) coated with equivalent film thicknesses of 165 nm for 3000 cycles and 40 nm for 733 cycles of TiO_2 ALD, respectively. Both samples display the formation of triangular patterns across the surface, revealing a universal behavior for templates with similar scalloped surfaces but different dimensions.

TiO_2 films were deposited for 733 cycles to a film thickness of ~40 nm on scalloped Al templates formed in oxalic acid. A tilted top-down SEM image of a thin delaminated film of TiO_2 retaining the original hexagonal pattern from the initial scalloped Al surface is shown in Figure 3a. However, the film's surface topography no longer displays the sharp peak structures that extruded from the initial, now-covered surface. A tilted bottom-up view of the delaminated film suggests the

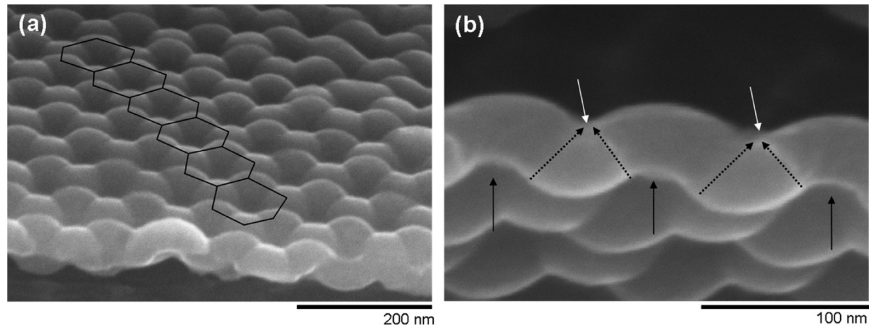

Figure 3. Delaminated conformal TiO_2 ALD film imaged in SEM: (a) tilted top-down view of merged growth fronts influenced by the hexagonal pattern of the removed underlying surface and (b) tilted bottom-up view of the film where dashed arrows in the cross section indicate where growth fronts merged and laterally moved due to film broadening at the peaks (solid black arrows) and causing the disappearance of the nanodimples (solid white arrows).

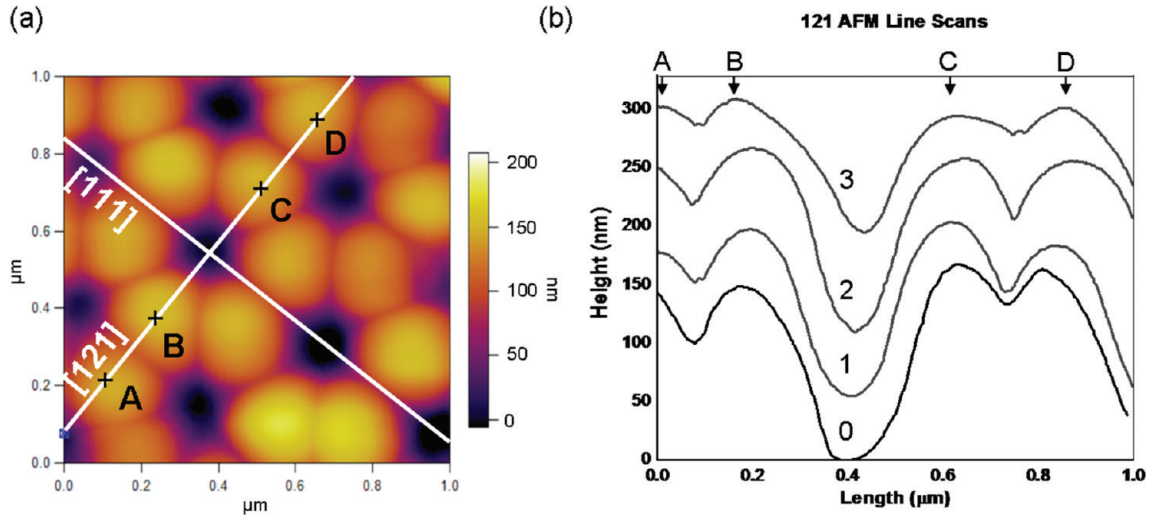

Figure 4. (a) AFM contour map of a 2000 cycle (~110 nm) TiO_2 ALD film on a scalloped Al surface dictating the [111] and [121] directions with peaks A, B, C, and D (denoted by +) across the template. (b) AFM line scans across the 121 direction after 0, 1000 (~ 55 nm), 2000 (~110 nm), and 3000 cycles (~165 nm) of deposited TiO_2 ALD (arrows denote locations of peaks). The profiles are numbered 0−3 for intervals of 1000 cycles each.

emergence of growth fronts for the evolving ALD film, where they eventually merged, as indicated by arrows in Figure 3b. As a TiO_2 film is conformally deposited over the original scalloped template, the ALD film topography changes shape with deposition and displays substantial smoothing of the original scalloped surface. This behavior underscores the benefits of conformal ALD to blunt or smooth sharp asperities and surface features with increasing film thickness. This is particularly important in some applications, for example, for local enhancement of electric fields at asperities and consequent low field breakdown of an MIM nanocapacitor.[1]

We attribute the display of growth fronts to the direct consequences of ALD conformality over surface topography that includes rounded as well as sloped regions. While other physical or chemical deposition mechanisms convey some measure of conformality over topography, ALD's self-limiting chemistry provides unprecedented capacity to maintain conformality even in the most challenging nanotopography. Side wall deposition (*i.e.*, on the inclined surfaces) is as rapid as on the rounded surfaces. This causes the rise of directional growth fronts where there is a significant change in incline on the surface (*i.e.*, shift from the sloped side walls to that of the concave valley or dimple). Growth fronts merge at crossing points between the inclined and curved regions and move laterally as deposition proceeds. When the initial surface comprises scalloped peaks and valleys that rise above lower dimples, the successive ALD layers exhibit changes in the surface profile, leading to the lateral growth and rounding of the peaks and reduction (or ultimately disappearance) of the valleys and lower dimple areas, as seen in Figure 3b.

This behavior is evident from AFM maps for ALD TiO_2 film profiles seen in Figure 4. TiO_2 films deposited on templates formed in phosphoric acid for 0 cycles, 1000 (55 nm), 2000 (110 nm), and 3000 cycles (165 nm) were mapped using AFM in order to monitor the progression of surface profiles and the decrease in surface area with increasing ALD film thickness. Figure 4a displays an AFM contour map for 2000 ALD cycles (110 nm), with the position of underlying peaks (A, B, C, and D) of the initial scalloped surface denoted along with the [121] and [111] directions. The map illustrates the emergence of triangular surface profiles as areas of higher topography allow growth fronts to extend out and finally merge along the [111] direction. AFM line scans taken of increased deposition across the [121] direction were layered and separated by the experimental growth rate for TiO_2, where 0, 1, 2, and 3 indicate the number of intervals for 1000 cycles, with 0 being the bare template (Figure 4b).

These results illustrate the broadening of peaks in the original scalloped surface initiated at positions A, B, C, and D. As neighboring peaks positioned at A and B as well as C and D expand, they first cause a sharpening of the valley between them and then begin to close and diminish the valley with further ALD coverage. At the location of the original dimples in the scalloped surface (*e.g.*, between B and C), much less of this effect is seen due to the lower plateau centered at the dimple being considerably wider to begin with. Ultimately, this behavior lends itself to the formation of the triangular pattern or nanopetunias across the surface. Although surface features of the samples were smaller than the AFM tips used, an increase in deposition indicates a decrease in surface area as growth fronts merge and the complex peak structure is rounded. ALD's ability to conformally coat and thereby modify a topographically rough surface will prove to be of great importance when engineering detailed geometries sometimes

found in 3D nanostructures. For example, ALD growth kinetics in high aspect ratio structures become primarily mass-transport-limited *via* molecule diffusion in and out of the pores rather than surface-reaction-limited.[12] Therefore, as the ALD deposition profile evolves, the entrance to a pore potentially found between B and C in Figure 4 will start to close off, creating an ever decreasing orifice diameter for molecules to diffuse through with each cycle and increasingly challenging ALD's ability to conformally deposit within a high aspect ratio nanopore.

A simple geometric 3D extrusion model was developed to demonstrate the influence of a complex surface topography and track the progression of ALD surface profiles. The model replicated the topography found on a scalloped Al template after removal of the PAA membrane by using the two key dimensions: interpore spacing, D_{int}, and the scallop's equivalent sphere radius, r_s. The interpore spacing of the scalloped array is a well-known dimension and is related to the anodization potential used for a specific anodization acid.[26] For the purpose of this simulation, D_{int} is taken as 105 nm corresponding to oxalic acid templates. The r_s value is the radius of curvature of the nanodimple imprinted in the Al surface and was extrapolated from AFM data of a bare scalloped Al surface. The maximum peak height was measured as the difference in the *z*-height between the bottom of the dimple and the top of the peak, which for a PAA surface anodized in oxalic acid at 40 V is approximately 42 nm. Knowing this value allows the surface to be modeled by adjusting r_s until the maximum ideal peak height is ~42 nm, which gives a value of $r_s \sim 65$ nm. Therefore, an ideal scalloped surface was coded in MatLab by spacing hemispheres with radius r_s in a hexagonal array, with intersphere spacing of D_{int} in the closed-pack direction and removing all intersecting data.

As mentioned earlier, much work already exists in the literature covering the strict theoretical modeling of ALD in terms of thickness as a function of cycles,[27] nucleation and growth kinetics,[28] and Monte Carlo simulations in ultrahigh aspect ratio nanopores.[14] For the purpose of our simulation, "ideal" ALD is assumed, where one monolayer of film is conformally deposited per cycle and ignores nucleation delays potentially present during the initial cycles of TiO_2 ALD on a removed PAA surface.[29] Instead, it uses experimentally determined growth rates and assumes that for each cycle the entire surface will be conformally coated with a specific amount of material given by the growth rate for the specified ALD process. The 2D cross-section schematic in Figure 5 depicts the step-by-step simulation sequence for a single ALD cycle. Starting with five equally spaced points on the initial surface (Figure 5a), surface normals were determined (Figure 5b). New data points were placed along each surface normal at a distance specified by the growth rate of the ALD process being simulated (Figure 5b). The new data points were no longer equally spaced along the *x*-axis; therefore, they were best fit with a new line (Figure 5c). A new set of equally spaced data points was created and placed along the best fit line, ultimately creating the new surface (Figure 5d).

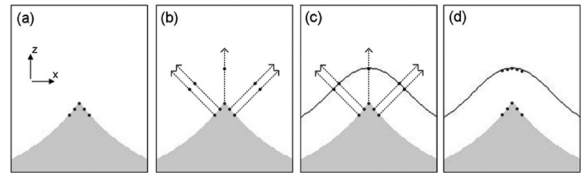

Figure 5. Geometric 3D extrusion model: (a) five equally spaced data points on the surface of a sharp peak. (b) Surface normals are projected out, and the data points for the new surface are placed along them using the prescribed growth rate; (c) the new data are fit with a "best fit" line; (d) the "best fit" line is used to generate more data, which are equally spaced in the *x*-direction.

The model described above used an initial surface prepared using oxalic acid and, therefore, cannot be directly compared with experimental results on a template prepared using phosphoric acid at 160 V. However, a similar scaling factor, *k*, used to compare film thicknesses from different templates can be used to compare the experimental results with the simulation, where D_{int} is 450 nm and $D^{o}_{int} = D_{sim} = 105$ nm. Top-view SEM images (Figure 6a−d) and top-view simulation results (Figure 6e−h) were compared, illustrating that the surface evolution of ALD on a scalloped Al surface mirrors what is seen in the extruded surface simulation.

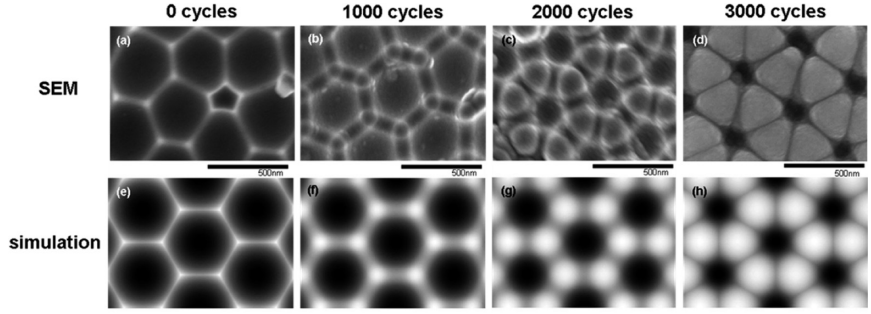

Figure 6. (a−d) Scalloped Al surface imaged in SEM after TiO_2 ALD deposition of 0, 1000 (~55 nm), 2000 (~110 nm), 3000 cycles (~165 nm); (e−h) simulation of surface evolution by extruding a model of the initial surface at the same rate as the deposition per cycle for ALD TiO_2.

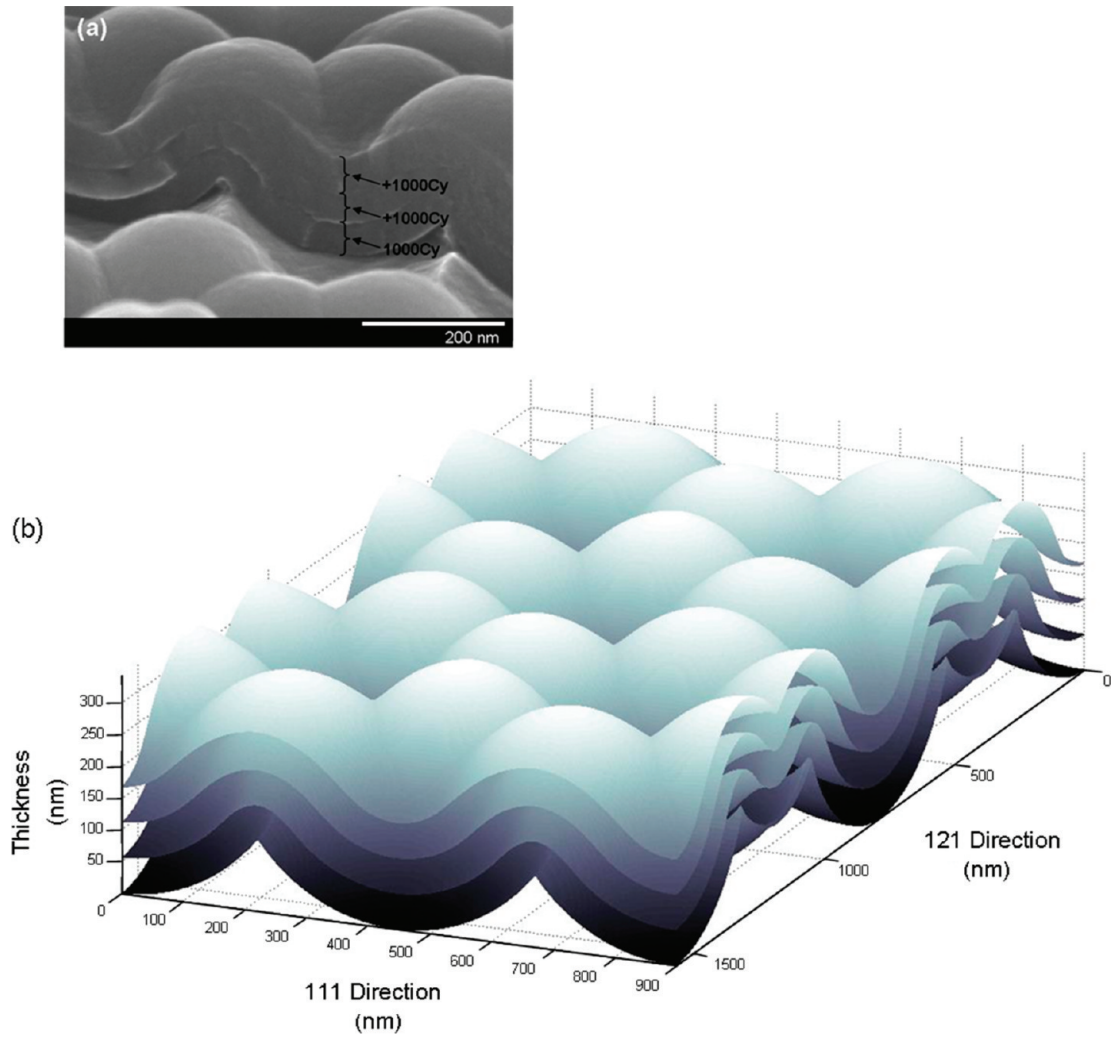

Figure 7. Cross-sectional surface profiles as a function of film thickness: (a) SEM image of three discontinuous 1000 cycle TiO_2 ALD films along the 111 direction of a scalloped Al surface and (b) modeled profiles of TiO_2 ALD films along the 111 and 121 directions of a scalloped Al surface.

Cross-sectional view SEM images along the [111] direction of a scalloped Al surface show three discrete 1000 cycle TiO_2 ALD films deposited one on top of another (Figure 7a). Each film set displays a distinct interface where the surface was exposed to air for *ex situ* characterization and indicates the presence of surface contamination. As deposition continued, films took on the form of the underlying film's surface, eventually creating a rounded knoll atop the initial peak in the Al template's surface, signifying there was no substantial topography-induced nucleation. Top-down and cross-sectional profiles along the [111] and [121] directions of the 3D model (Figure 7b) re-emphasize that ALD deposits in a conformal manner and that the formation of triangular islands seen in both SEM images and the 3D model is an artifact of the underlying surface and not due to nucleation and growth resonating from the tips of the sharp peaks. Raman data, to be published elsewhere, further revealed that films were amorphous.

Surface area plays an integral part in the design and nanofabrication of next generation energy devices, such as MIM nanocapacitors. Matlab simulations were used to estimate the change in surface area as a function of film thickness. The surface area was estimated by summing the areas of all the quadrilaterals that comprise the modeled surface as defined by the *X*, *Y*, *Z* coordinate data. The planar equivalent area is the 2D surface equivalence to the area projected onto the *XY* plane from the 3D model. From these estimations, the initial surface of a template formed in oxalic acid was estimated to have a 30% larger area than its planar equivalent. Templates formed in phosphoric acid would have smaller surface areas due to larger interpore spacings, meaning there are fewer peaks for the same planar area used above. Starting with the initial surface of the scalloped Al template, an ALD simulation was performed for 1000 cycles with a growth rate of 0.1 nm/cycle. The normalized surface area (the estimated surface area divided by the planar equivalent surface area) as a function of ALD film thickness was plotted with corresponding 3D representations of the evolving surface profile (Figure 8). As the deposition proceeds, the

normalized surface does not change appreciably until after ~45 nm. After 45 nm of film growth, the normalized surface area asymptotically decays toward a limiting value of 1, implying that the surface has been effectively "planarized". The shoulder at 45 nm seems to coincide with the appearance of lines in the film where film growth fronts have started to merge along the [111] direction of the hexagonal scalloped cell (see Figure 8). This is the moment at which the curvature of the saddle points between the peaks in the scalloped surface is completely inverted by the continued extrusion of the ALD deposition over the sharp peaks. Further deposition results in the extension of these lines toward the center of the scallops further unifying the surface.

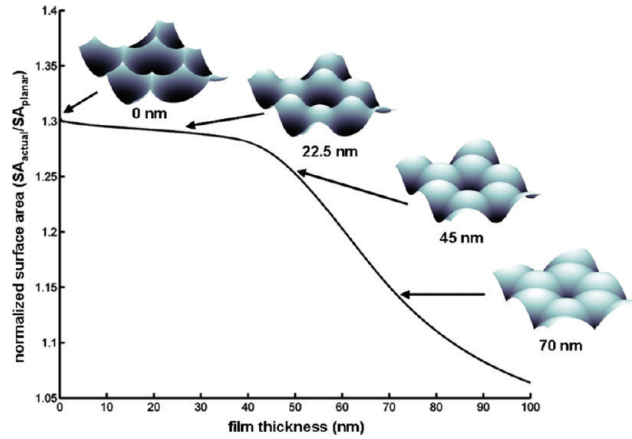

Figure 8. Normalized surface area as a function of ALD film thickness.

CONCLUSIONS

TiO_2 ALD films were deposited on a highly scalloped Al surface to demonstrate the ability of ALD to provide exceedingly conformal films over a complex topography of a template's initial surface. SEM images and AFM scans reveal the progression of triangular surface profiles that change with ALD layer thickness, influenced by the way ALD conformally coats the underlying topography, and further emphasizing that ALD nucleation is rather insensitive to the surface topography at least for the experimental process chemistry investigated here.

We demonstrated the usefulness of a simple geometric 3D extrusion model to simulate the evolution of ALD films' surface profiles as they conformally coat the complex surface topography of a modeled scalloped Al surface. The scalloped Al surface was modeled and calibrated using dimensions extracted from SEM and AFM scans. The surface was then extruded in a stepwise manner using experimentally obtained growth rates of the particular ALD chemistry being simulated. The model illustrates how conformal ALD films cause the surface topography to change with each deposited layer, ultimately leading to a decrease in surface area as a function of film thickness. Results from this model and experimental data are in excellent agreement, leading to the conclusion that no nucleation-related effects were observed and the resulting triangular pattern is an artifact of the underlying textured Al surface.

This work illustrates the benefits of ALD to conformally coat and manipulate surface topographies in which sharp asperities or nanoroughness could potentially limit device performance. Ultimately this work will play an important role in the design and nanofabrication of devices which exploit nanoprocesses such as PAA and ALD.

MATERIALS AND METHODS

Scalloped aluminum templates were synthesized by the removal of PAA membranes formed during a one-step anodization method.[30] High purity 200 μm thick aluminum foils (99.99%, Alfa Aesar) were electropolished in a 1:5 perchloric acid/ethanol bath held at ~3 °C in order to remove microroughness from the surface, which influences the quality of the pores. The electropolished aluminum was then anodized at (1) 40 V and 10 °C in an electrolytic bath of 0.3 M oxalic acid to achieve an interpore spacing, D_{int}, of 110 nm or (2) 160 V and 4 °C in an electrolytic bath of 10 wt % phosphoric acid to achieve D_{int} of 450 nm. Foils were anodized for ~7 h so PAA pores would self-organize and align orthogonally with respect to the underlying Al substrate. After anodization, the PAA film produced was removed in an aqueous solution of phosphoric acid (6 wt %) and chromic acid (1.8 wt %) at 60 °C, leaving a hexagonally organized nanodimple array with a highly scalloped surface imprinted in the remaining aluminum.

Titanium dioxide (TiO_2) ALD thin films were thermally deposited at 150 °C in a Beneq TFS-500 cross-flow ALD reactor using tetrakis(dimethylamido)titanium (TDMAT) and water. Pulses and purges of 500 ms for both precursors resulted in atomic thickness control with a growth rate of 0.055 nm/cycle as a submonolayer of film was consistently deposited for each cycle. Three samples were loaded during the first run, and deposition was carried out in three intervals of a fixed number of cycles (*i.e.*, 244 or 1000 for templates anodized in oxalic or phosphoric acid, respectively). After each interval, one sample was removed from the reactor and characterized *via* high-resolution scanning electron microscopy (SEM, Hitachi SU-70) and atomic force microscopy (AFM, MFP-3D Asylum Research) in tapping mode. Film growth rates were determined using a spectroscopic ellipsometer (Sopra GES5) on planar Si samples.

Acknowledgment. This work has been partially supported by the Laboratory for Physical Sciences and by the UMD-NSF-MRSEC under Grant DMR 05-20471. The authors would like to thank J. Seog and W. Hwang for the use and help with AFM, the Nano-Center and the NISP Lab at the University of Maryland for materials processing and characterization, and MKS Instruments and Inficon Inc. for continued support of research activities in the lab.

REFERENCES AND NOTES

1. Banerjee, P.; Perez, I.; Henn-Lecordier, L.; Lee, S. B.; Rubloff, G. W. Nanotubular Metal−Insulator−Metal Capacitor Arrays for Energy Storage. *Nat. Nanotechnol.* **2009**, *4*, 292–296.
2. Liu, R.; Lee, S. B. MnO_2/Poly(3,4-ethylenedioxythiophene) Coaxial Nanowires by One-Step Coelectrodeposition for

Electrochemical Energy Storage. *J. Am. Chem. Soc.* **2008**, *130*, 2942–2943.
3. Pellin, M. J.; Stair, P. C.; Xiong, G.; Elam, J. W.; Birrell, J.; Curtiss, L.; George, S. M.; Han, C. Y.; Iton, L.; Kung, H.; *et al.* Mesoporous Catalytic Membranes: Synthetic Control of Pore Size and Wall Composition. *Catal. Lett.* **2005**, *102*, 127–130.
4. Elam, J. W.; Zinovev, A.; Han, C. Y.; Wang, H. H.; Welp, U.; Hryn, J. N.; Pellin, M. J. Atomic Layer Deposition of Palladium Films on Al_2O_3 Surfaces. *Thin Solid Films* **2006**, *515*, 1664–1673.
5. Artzi-Gerlitz, R.; Benkstein, K. D.; Lahr, D. L.; Hertz, J. L.; Montgomery, C. B.; Bonevich, J. E.; Semancik, S.; Tarlov, M. J. Fabrication and Gas Sensing Performance of Parallel Assemblies of Metal Oxide Nanotubes Supported by Porous Aluminum Oxide Membranes. *Sens. Actuators, B* **2009**, *136*, 257–264.
6. Elam, J. W.; Xiong, G.; Han, C. Y.; Wang, H. H.; Birrell, J. P.; Welp, U.; Hryn, J. N.; Pellin, M. J.; Baumann, T. F.; Poco, J. F.; *et al.* Atomic Layer Deposition for the Conformal Coating of Nanoporous Materials. *J. Nanomater.* **2006**, 1–5.
7. Im, H.; Lindquist, N. C.; Lesuffleur, A.; Oh, S. H. Atomic Layer Deposition of Dielectric Overlayers for Enhancing the Optical Properties and Chemical Stability of Plasmonic Nanoholes. *ACS Nano* **2010**, *4*, 947–954.
8. Gerritsen, E.; Emonet, N.; Caillat, C.; Jourdan, N.; Piazza, M.; Fraboulet, D.; Boeck, B.; Berthelot, A.; Smith, S.; Mazoyer, P. Evolution of Materials Technology for Stacked-Capacitors in 65 nm Embedded-DRAM. *Solid-State Electron.* **2005**, *49*, 1767–1775.
9. Rosenberg, R.; Edelstein, D. C.; Hu, C. K.; Rodbell, K. P. Copper Metallization for High Performance Silicon Technology. *Annu. Rev. Mater. Sci.* **2000**, *30*, 229–262.
10. Wilk, G. D.; Wallace, R. M.; Anthony, J. M. High-Kappa Gate Dielectrics: Current Status and Materials Properties Considerations. *J. Appl. Phys.* **2001**, *89*, 5243–5275.
11. Manoj, C. R.; Rao, V. R. Impact of High-K Gate Dielectrics on the Device and Circuit Performance of Nanoscale FinFETS. *IEEE Electron Device Lett.* **2007**, *28*, 295–297.
12. Gordon, R. G.; Hausmann, D.; Kim, E.; Shepard, J. A Kinetic Model for Step Coverage by Atomic Layer Deposition in Narrow Holes or Trenches. *Chem. Vap. Deposition* **2003**, *9*, 73–78.
13. Gates, S. M. Surface Chemistry in the Chemical Vapor Deposition of Electronic Materials. *Chem. Rev.* **1996**, *96*, 1519–1532.
14. Elam, J. W.; Routkevitch, D.; Mardilovich, P. P.; George, S. M. Conformal Coating on Ultrahigh-Aspect-Ratio Nanopores of Anodic Alumina by Atomic Layer Deposition. *Chem. Mater.* **2003**, *15*, 3507–3517.
15. Leskela, M.; Ritala, M. Atomic Layer Deposition (ALD): From Precursors to Thin Film Structures. *Thin Solid Films* **2002**, *409*, 138–146.
16. Niinisto, L.; Paivasaari, J.; Niinisto, J.; Putkonen, M.; Nieminen, M. Advanced Electronic and Optoelectronic Materials by Atomic Layer Deposition: An Overview with Special Emphasis on Recent Progress in Processing of High-K Dielectrics and Other Oxide Materials. *Phys. Status Solidi A* **2004**, *201*, 1443–1452.
17. Masuda, H.; Yamada, H.; Satoh, M.; Asoh, H.; Nakao, M.; Tamamura, T. Highly Ordered Nanochannel-Array Architecture in Anodic Alumina. *Appl. Phys. Lett.* **1997**, *71*, 2770–2772.
18. Martinson, A. B. F.; Elam, J. W.; Hupp, J. T.; Pellin, M. J. ZnO Nanotube Based Dye-Sensitized Solar Cells. *Nano Lett* **2007**, *7*, 2183–2187.
19. Zhou, Y. K.; Shen, C. M.; Li, H. L. Synthesis of High-Ordered $LiCOO_2$ Nanowire Arrays by AAO Template. *Solid State Ionics* **2002**, *146*, 81–86.
20. Masuda, H.; Hasegwa, F.; Ono, S. Self-Ordering of Cell Arrangement of Anodic Porous Alumina Formed in Sulfuric Acid Solution. *J. Electrochem. Soc.* **1997**, *144*, L127–L130.
21. Edgar, J. H.; Du, L.; Nyakiti, L.; Chaudhuri, J. Native Oxide and Hydroxides and Their Implications for Bulk AlN Crystal Growth. *J. Cryst. Growth* **2008**, *310*, 4002–4006.
22. Kim, H.; Lee, H. B. R.; Maeng, W. J. Applications of Atomic Layer Deposition to Nanofabrication and Emerging Nanodevices. *Thin Solid Films* **2009**, *517*, 2563–2580.
23. Gobbert, M. K.; Prasad, V.; Cale, T. S. Predictive Modeling of Atomic Layer Deposition on the Feature Scale. *Thin Solid Films* **2002**, *410*, 129–141.
24. Leskela, M.; Kemell, M.; Kukli, K.; Pore, V.; Santala, E.; Ritala, M.; Lu, J. Exploitation of Atomic Layer Deposition for Nanostructured Materials. *Mater. Sci. Eng. C* **2007**, *27*, 1504–1508.
25. Asoh, H.; Nishio, K.; Nakao, M.; Tamamura, T.; Masuda, H. Conditions for Fabrication of Ideally Ordered Anodic Porous Alumina Using Pretextured Al. *J. Electrochem. Soc.* **2001**, *148*, B152–B156.
26. Lee, W.; Ji, R.; Gosele, U.; Nielsch, K. Fast Fabrication of Long-Range Ordered Porous Alumina Membranes by Hard Anodization. *Nat. Mater.* **2006**, *5*, 741–747.
27. Xie, Q.; Musschoot, J.; Deduytsche, D.; Van Meirhaeghe, R. L.; Detavernier, C.; Van den Berghe, S.; Jiang, Y. L.; Ru, G. P.; Li, B. Z.; Qu, X. P. Growth Kinetics and Crystallization Behavior of TiO_2 Films Prepared by Plasma Enhanced Atomic Layer Deposition. *J. Electrochem. Soc.* **2008**, *155*, H688–H692.
28. Elam, J. W.; Nelson, C. E.; Grubbs, R. K.; George, S. M. Nucleation and Growth during Tungsten Atomic Layer Deposition on SiO_2 Surfaces. *Thin Solid Films* **2001**, *386*, 41–52.
29. Xie, Q.; Jiang, Y. L.; Detavernier, C.; Deduytsche, D.; Van Meirhaeghe, R. L.; Ru, G. P.; Li, B. Z.; Qu, X. P. Atomic Layer Deposition of TiO_2 from Tetrakis-Dimethyl-Amido Titanium or Ti Isopropoxide Precursors and H_2O. *J. Appl. Phys.* **2007**, *102*, 083521(1)083521(6) .
30. Masuda, H.; Satoh, M. Fabrication of Gold Nanodot Array Using Anodic Porous Alumina as an Evaporation Mask. *Jpn. J. Appl. Phys.* **1996**, *35*, L126–L129.